N95-21542

TDA Progress Report 42-120

February 15, 1995

The Efficiency Calibration of the DSS-24 34-Meter Diameter Beam-Waveguide Antenna

L. S. Alvarez, M. J. Britcliffe, M. M. Franco, S. R Stewart, and H. J. Jackson
Ground Antennas and Facilities Engineering Section

Microwave performance testing of the new Deep Space Station (DSS)-24 34-m-diameter antenna was carried out during the summer of 1994. Efficiency measurements were made at the 8.45-GHz (X-band) and 32-GHz (Ka-band) frequencies both at the antenna Cassegrain (f1) and beam-waveguide (f3) focal points. In addition, the antenna f3 efficiencies were measured on the DSS-24 operational 2.295-GHz (S-band) and 8.45-GHz feeds. This article presents the efficiency determinations as a function of elevation angle along with a corresponding error analysis of the measurements. Peak measured gains and efficiencies are tabulated for all frequencies.

I. Introduction

During an 8-week period in the summer of 1994, extensive microwave performance measurements were carried out on the new Deep Space Station (DSS)-24 34-m beam-waveguide (BWG) antenna at Goldstone, California. The testing period consisted of antenna efficiency and pointing calibration and system noise temperature measurements at the frequencies of 2.295 GHz (S-band), 8.45 GHz (X-band), and 32 GHz (Ka-band).[1] In addition, microwave holography and subsequent main antenna reflector-panel adjustments were carried out at the Cassegrain (f1) focus before the start of the efficiency calibration period. The X- and Ka-band efficiency measurements involved the use of portable microwave test packages installed at the f1 focal point and the subterranean f3 beam-waveguide focal point. The test packages were previously developed for testing of the DSS-13 research and development (R&D) antenna.[2] In addition to the measurements on the R&D feeds, the performances of the DSS-24 operational S- and X-band feeds were also characterized at the f3 focal point.

This article presents the efficiency calibration and analysis portion of the microwave DSS-24 testing. The methodology used to determine the antenna aperture efficiency from noise temperature measurements on radio source calibrators is reviewed and error analysis equations are presented. The following sections then present the results of the efficiency determination at the f1 and f3 focal points, with discussion of

[1] The testing period is described in detail in *DSS-24 Microwave Performance Characterization*, Document 829-6 (internal document), Jet Propulsion Laboratory, Pasadena, California, May 15, 1994.

[2] M. J. Britcliffe, L. S. Alvarez, D. A. Bathker, P. W. Cramer, T. Y. Otoshi, D. J. Rochblatt, B. L. Seidel, S. D. Slobin, S. R. Stewart, W. Veruttipong, and G. E. Wood, *DSS 13 Beam-Waveguide Antenna Project: Phase 1 Final Report*, JPL D-8451 (internal document), Jet Propulsion Laboratory, Pasadena, California, May 15, 1991.

the particular circumstances of each measurement set and the data analysis. The final section presents a summary of the peak gains and efficiencies measured during the testing period.

II. Efficiency Calibration Methodology

A. Efficiency Determination

Determination of the DSS-24 aperture efficiency follows a previously developed methodology [1].[3] Peak radio-source noise temperatures are measured at different antenna orientations via a boresight (actually a step-scan) algorithm [2] resident in a PC-based radiometer system. This automated boresighting program, know as AUTOBORE, was previously developed for performance testing of DSS 13 [3].

To yield an estimate of antenna efficiency, these measured quantities are then normalized by the absolute source calibration temperature, $T_a = T_{100}/C_r$, where T_{100} is the 100-percent antenna efficiency temperature computed from the best-known radio source flux density and C_r is the source size correction factor (see [1] and [4] for more details).[4]

For this article, the aperture efficiency measured at DSS 24 is referenced to the input of the low-noise amplifier and, thus, includes the losses of the feed system. In equation form, the efficiency, $\eta(el)$, for a given elevation angle, el, as measured on site is

$$\eta(el) = \frac{T_p(el)}{T_a} \tag{1}$$

where T_p is the peak on-source temperature. The effects of atmospheric attenuation must be considered; then the Eq. (1) becomes

$$\eta(el) = \frac{L(el)T_p(el)}{T_a} \tag{2}$$

where $L(el)$ is the atmospheric attenuation loss factor, which is described below.

B. Correction for Atmospheric Attenuation

In order to report the DSS-24 efficiency without the effects of atmospheric absorption, the estimated source peak temperatures from the antenna boresight measurements must be scaled up by a computed loss factor. A computer program, SDSATM4S.BAS,[5] is used to estimate total zenith attenuation values, A_{zen}, from surface measurements of temperature, pressure, and relative humidity. From A_{zen}, the attenuation loss factor for the logged boresight elevation angles can then be calculated. For clarity, the equations for the computation given in [1] are repeated here. The attenuation at elevation angle el is computed from

$$A(el) = \frac{A_{zen}}{\sin(el)} \tag{3}$$

where A_{zen} is in units of decibels. The radio source peak temperature, in a vacuum condition, is defined by

---

[3] Ibid.

[4] Values of the temperature $T_a = T_{100}/C_r$ for radio sources used to calibrate DSN antennas are given in P. Richter, *DSN Radio Source List for Antenna Calibration*, JPL D-3801, Rev. C (internal document), Jet Propulsion Laboratory, Pasadena, California, August 19, 1993.

[5] Courtesy of S. Slobin, Telecommunications Systems Section, Jet Propulsion Laboratory, Pasadena, California.

$$T_{p,v}(el) = L(el)T_p(el) \tag{4}$$

where $T_p(el)$ is the actual peak source temperature output from the boresight measurement, and the loss factor, $L(el)$, is given by

$$L(el) = 10^{(A(el)/10)} \tag{5}$$

C. Error Analysis

From Eq. (2), the variance of the efficiency, σ_η^2, may be expressed as

$$\left(\frac{\sigma_{\eta(el)}}{\eta(el)}\right)^2 = \left(\frac{\sigma_{T_a}}{T_a}\right)^2 + \left(\frac{\sigma_{T_p}}{T_p(el)}\right)^2 + \left(\frac{\sigma_{L(el)}}{L(el)}\right)^2 \tag{6}$$

where σ_{T_a}, σ_{T_p}, and σ_L are, respectively, the uncertainties of the absolute calibration source temperature, the measured source temperature, and the atmospheric attenuation loss factor. It can be shown that propagation of the loss factor, $L(el)$, with respect to the zenith attenuation value, A_{zen}, from Eq. (5) results in

$$\left(\frac{\sigma_{L(el)}}{L(el)}\right)^2 = (\ln(10)\log(L(el)))^2 \left(\frac{\sigma_{A_{zen}}}{A_{zen}}\right)^2 \tag{7}$$

which, inserted into Eq. (6), yields the efficiency variance function as

$$\left(\frac{\sigma_{\eta(el)}}{\eta(el)}\right)^2 = \left(\frac{\sigma_{T_a}}{T_a}\right)^2 + \left(\frac{\sigma_{T_p}}{T_p(el)}\right)^2 + (\ln(10)\log(L(el)))^2 \left(\frac{\sigma_{A_{zen}}}{A_{zen}}\right)^2 \tag{8}$$

A term-by-term computation of the error variance follows. The values of the pair (T_a, σ_{T_a}) for various radio source calibrators are taken from Richter[6] for a 34-m antenna at each of the S-, X-, and Ka-frequency bands. The magnitude of the efficiency calibration is directly dependent on the value of T_a and its accuracy. The uncertainty, σ_{T_p}, is obtained from the residual sum of squares of the best-fit quadratic curve to the peak noise temperature samples, $T_p(el)$, versus elevation angle. It is an estimate of the on-source radiometer measurement noise and is assumed to be constant with respect to time and elevation angle. The loss factor uncertainty, $\sigma_L(el)$, is computed from a probable error of 10 percent on the zenith attenuation value,[7] i.e., $\sigma_{Azen} = 0.1A_{zen}$. Note that since A_{zen} is calculated from surface weather measurements, it is a time-varying quantity. However, the error statistic $\sigma_{A_{zen}}$ is modeled as stationary. For the DSS-24 calibration period, values for A_{zen} are computed and analyzed using weather instrumentation recordings from DSS 24 (mounted on the microwave front-end test package itself), DSS 13, and Signal Processing Center (SPC) 10.

Lastly, it is assumed that there is no systematic efficiency loss due to beam-pointing errors during the boresight measurements since the algorithm is continually updating antenna-pointing corrections. Also, systematic efficiency losses due to errors in subreflector focusing and beam-waveguide mirror misalignments are, when applicable, added to the computed value of σ_η.

---

[6] P. Richter, op. cit.

[7] Personal communication with S. Slobin, op. cit., August 1994.

III. Radio Source Calibration Values

At all of the frequency bands, S-, X- and Ka-bands, the radio source 3C274 (Virgo A) is used as the principal calibrator. Due to a constrained time schedule during the radio frequency (rf) performance evaluation period, the main measurement strategy consisted of first obtaining a full track of 3C274 (rise to set) to establish the peak efficiency near the rigging angle (40–50 deg). Since 3C274 is only near a 12-deg declination, higher declination sources (3C84 and 3C123) are then tracked to establish the upper efficiency curve. For the X- and Ka-bands, the efficiency curves generated for these latter sources are normalized to the measured 3C274 peak value.

Table 1 summarizes the flux, source size correction values, calibration temperatures $T_a = T_{100}/C_r$, and the estimated uncertainties for the radio sources 3C274 and 3C123 (the latter is used for calibration at S-band only). These values are taken directly from Richter[8] and are calculated for a DSN 34-m antenna with half-power beamwidths of 0.240 deg for S-band, 0.063 deg for X-band, and 0.017 deg for Ka-band. The uncertainties are used in the error analysis of the efficiency calculations.

Table 1. Radio sources used for DSS-24 efficiency calibration.

Source and frequency, GHz	Flux density, Janskys	C_r	T_a, K	T_a 1-sigma, K
3C274 at 8.42	44.69	1.087	13.518	0.324
3C274 at 32	16.22	1.270	4.200	0.130
3C274 at 2.295	137.24	1.060	42.570	1.022
3C123 at 2.295	31.00	1.000	10.190	0.245

IV. Efficiency Measurements: X-Band at f1

The X-band efficiency measurements were made at the f1 focal point with the R&D feed package. As these were the first measurements made after holography, all of the star tracks applied the holography-determined best 45-deg subreflector offsets (in the y- and z-axis). These offsets are superimposed onto the structural (elevation-dependent) predict curves resident in the antenna-pointing controller (APC). No pointing model was used during the f1 X-band tracks. However, subsequent analysis of the pointing errors (relative to the last boresight) indicated that no more than 0.002 deg of total pointing error was built up between the peak noise temperature estimates. This resulted in only a very small gain loss ($\approx$ 0.01 dB for a 0.063-deg X-band full-width half-power beamwidth) and, hence, measurements from the first two star tracks on 3C274 and 3C84 were used for efficiency calculation.

The zenith attenuation values for the 2-day tracking period (DOY 144–145) varied from 0.036 to 0.042 dB. The best-fit efficiency curve and the adjusted data points are shown in Fig. 1. The peak X-band efficiency at f1 was determined to be 75.25 percent at an elevation angle of 42.5 deg. Using Eq. (8), the one–standard deviation uncertainty on the best-fit peak efficiency is computed to be 2.04 percent. The peak X-band efficiency and uncertainty correspond to a peak gain of 68.33 dBi $\pm$ 0.12 dB. The uncertainty on the efficiency below 30-deg elevation is greater due to insufficient (and nonrepeatable) measurement points available for the curve fit. At 20 deg, the one–standard deviation error is estimated to be 3 percent.

[8] P. Richter, op. cit.

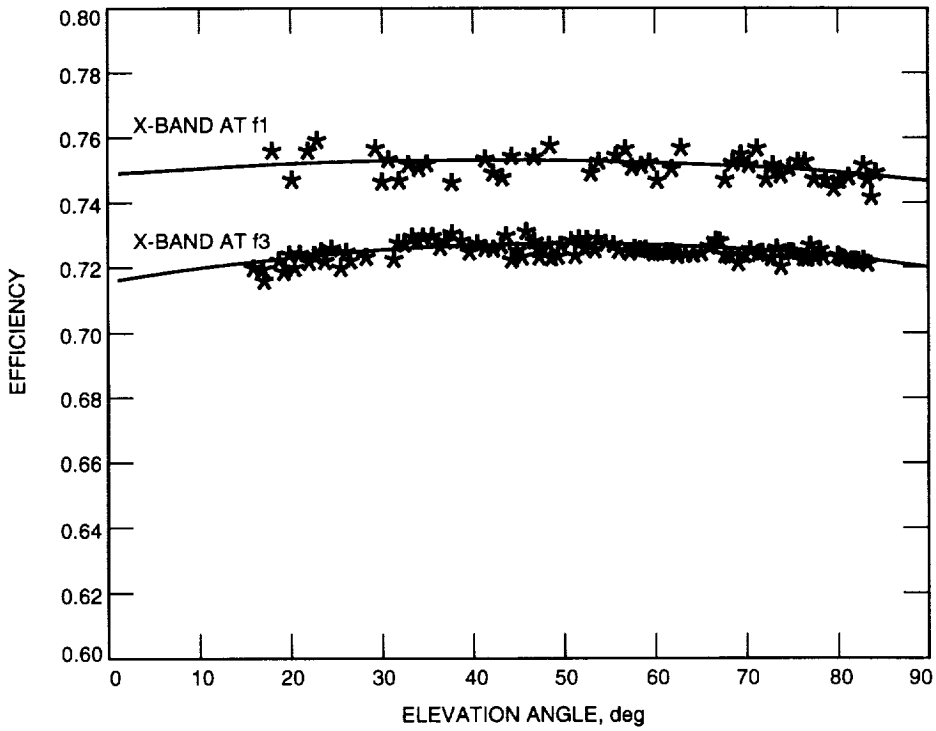

Fig. 1. DSS-24 8.45-GHz efficiency at the f1 and f3 focal points, without atmosphere.

V. Efficiency Measurements: X-Band at f3

X-band efficiency measurements at the f3 focal point were taken over 5 days (DOY 174–178) using the R&D microwave test package. Following the general data-taking strategy, the sources 3C274 and 3C84 were tracked until efficiency curves could be computed on each source. The peak efficiency on the variable source 3C84 was then normalized to the peak 3C274 value. All of the measurements were compensated for atmospheric absorption on a point-by-point basis. For the final 2 days of tracking, the computed zenith attenuation values ranged only from 0.0334 to 0.035 dB. The best-fit efficiency curve based on these final days and the adjusted measurements is shown in Fig. 1.

The peak X-band efficiency at f3 was calculated to be 72.67 percent at an elevation angle of 49 deg. From Eq. (8), the computed uncertainty on the peak efficiency is 1.81 percent. The peak X-band efficiency and uncertainty at f3 correspond to a peak gain of 68.19 dBi $\pm$ 0.11 dB. As seen in Fig. 1, the efficiency data points taken on the two radio sources are numerous and repeatable over the elevation range. The uncertainty estimate of 1.81 percent is assumed constant with elevation angle since the last two error contributors (measurement noise and attenuation errors) in Eq. (8) contribute less than 10 percent to the total. As will be discussed below, radiometry techniques were applied to derive a total subreflector offset curve for use at Ka-band at f3 that differed from that used during the above X-band tracks and the Ka-band f1 tracks. However, the effects on the presented X-band efficiency results are negligible.

VI. Efficiency Measurements: Ka-Band at f1

The Ka-band R&D microwave test package was used for efficiency calibration at both the DSS-24 f1 and f3 focal points. At f1, just over a week was devoted to star tracks at Ka-band. The tracks from the first days, combined with the previous X-band boresight data, yielded the first pointing model for the antenna. This was requisite in order to keep the scan-to-scan error in each axis under 0.001 deg (resulting

at most in an $\approx$ 0.08-dB pointing loss for a 0.017-deg Ka-band full-width half-power beamwidth). A 0.001-deg upper bound on the tracking error in each axis was a practical calibration goal given that the pointing-error measurement accuracy was not expected to be much better than 0.001 deg due to the low signal-to-noise operating conditions during radio source tracking. In addition to beam-pointing calibration, approximately 3 days were also devoted to obtaining the best subreflector offset positioning during the efficiency measurements. The optimization procedure, based on manually entering subreflector offsets into the APC in between boresights and postprocessing the output data together with the structural predict models, yielded the total f1 offset curves shown in Fig. 2. These new focusing curves were then used for the remainder of the f1 testing. The final 2 days of tracking (DOY 158 and 159) resulted in sufficient data points on 3C274 and 3C84 for the efficiency calibration curve.

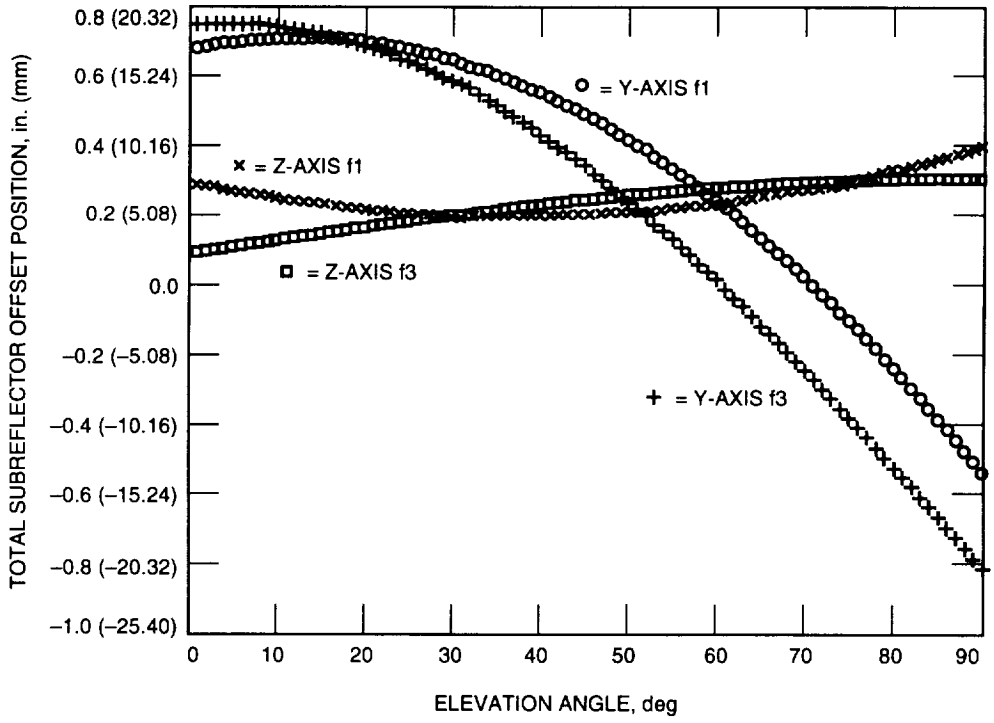

Fig. 2. Subreflector position offset curves used during Ka-band measurements at f1 and f3.

The effects of the atmospheric attenuation become more significant with increasing frequency band. For this reason, the logged weather readings were closely reviewed. Figure 3 shows the computed 32-GHz zenith attenuation values for DOY 158, based on weather data logged at DSS 24 (sensors mounted on the X-band test package on the ground), and from readings logged daily at DSS 13 and SPC 10. In Fig. 3, the SPC-10 and DSS-13 values for A_{zen} show good agreement, but the data points for DSS 24 appear inconsistent, indicating a problem with the local sensors. Note that the readings at DSS 24 were logged only during the tracking periods. Since DSS 24 is closer in location to SPC 10 than to DSS 13, the SPC-10 weather data were used to remove the effects from the efficiency measurements. As seen in Fig. 3, the values for A_{zen} varied from 0.11 to 0.16 dB during the course of the star tracks. The best-fit efficiency curve and the adjusted data points for Ka-band at f1 are shown in Fig. 4.

The Ka-band peak efficiency at f1 was calculated to be 60.60 percent at an elevation angle of 44.5 deg. From Eq. (8), the uncertainty estimate for the efficiency measurements was computed for all elevation angles. A plot of the uncertainty ratio $\sigma_{\eta(el)}/\eta(el)$ on the efficiency data is shown in Fig. 5. As expected, the error in measuring the efficiency is minimum at 45-deg elevation, where the measured source noise

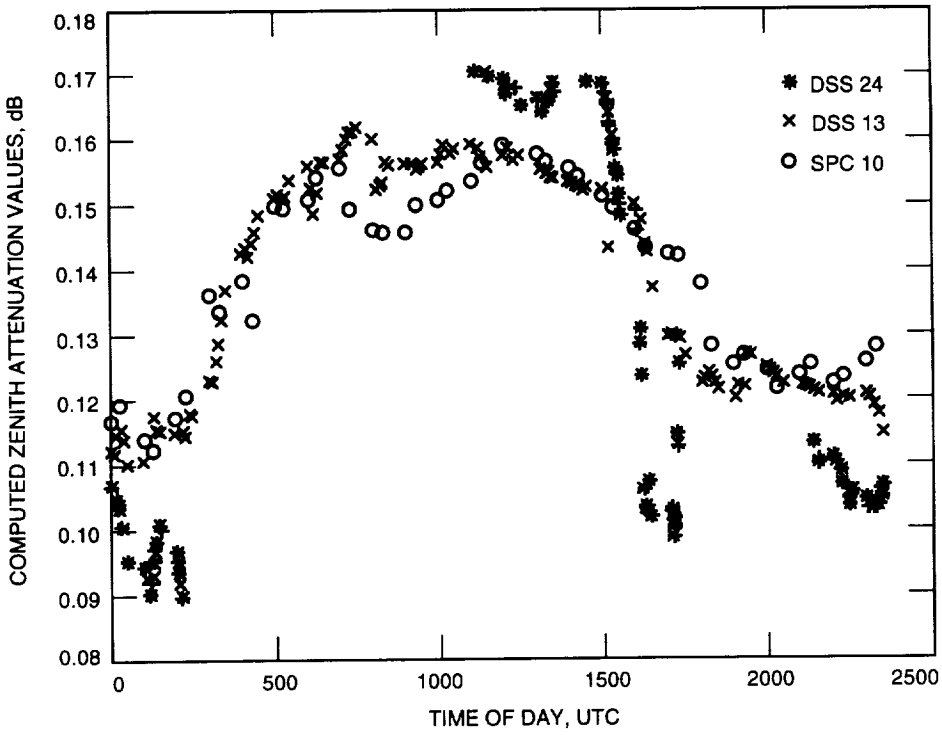

Fig. 3. Computed 32-GHz zenith attenuation values for DOY 158.

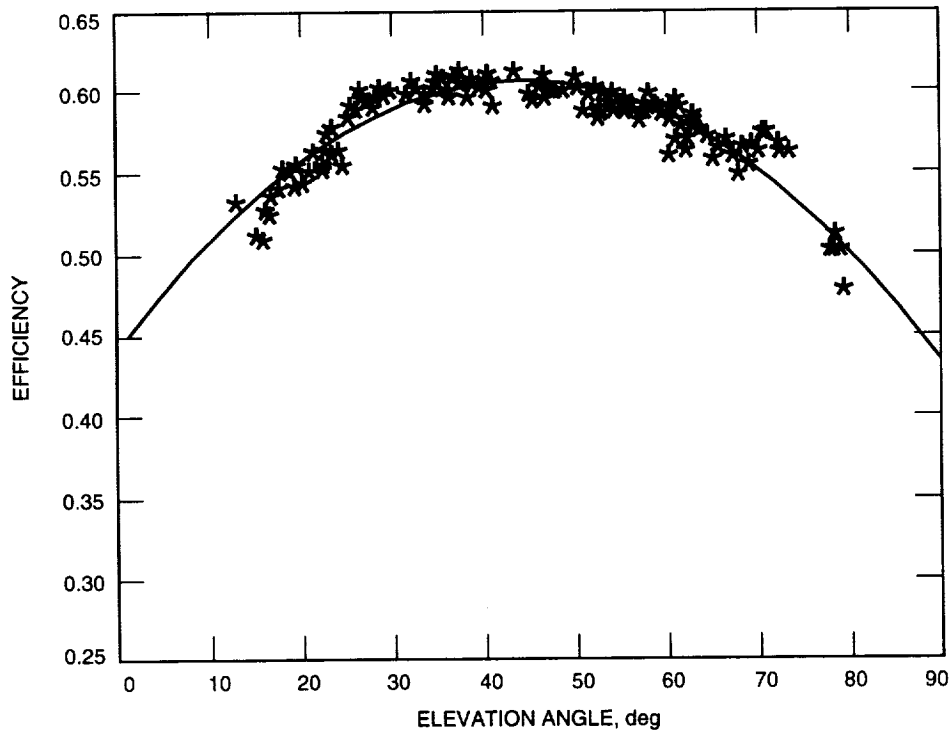

Fig. 4. DSS-24 32-GHz efficiency at the f1 focal point, without atmosphere.

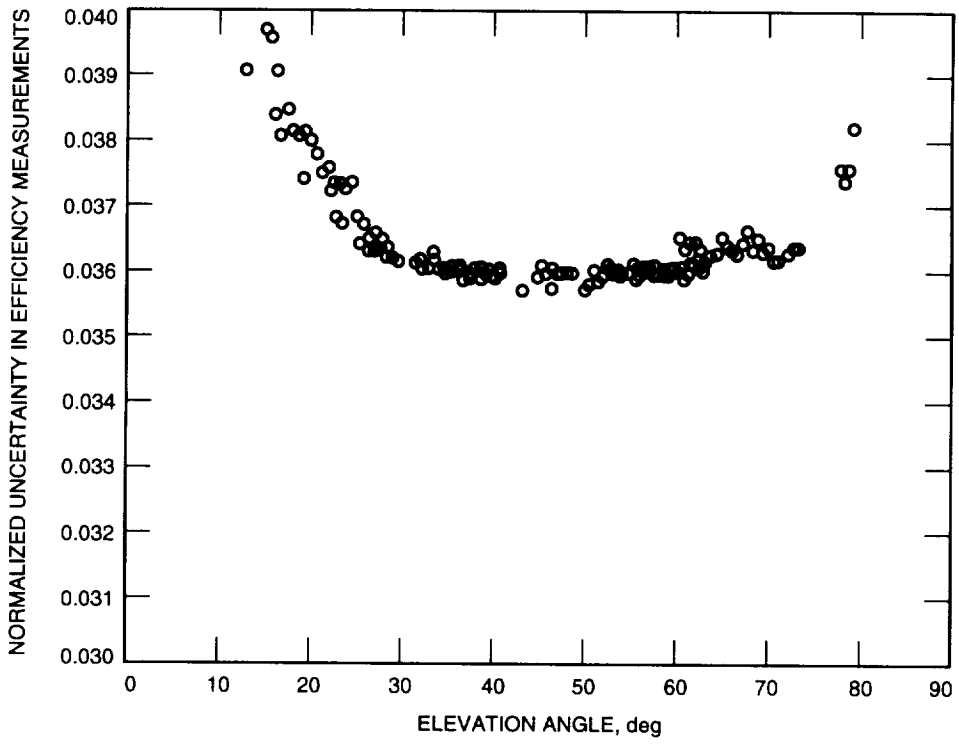

Fig. 5. DSS-24 32-GHz normalized efficiency uncertainty ($\sigma_\eta(el)/\eta(el)$) at the f1 focal point, without atmosphere.

temperature is maximum (i.e., the largest signal-to-noise ratio condition). The uncertainty ratio increases when the elevation angle deviates from the rigging angle since the efficiency decreases due to gravity, and the largest magnitude is at the lower elevations due to the increased atmospheric attenuation variance $\sigma^2_{L(el)}$. The one–standard deviation uncertainty σ_η on the peak efficiency of 60.60 percent at 44.5 deg is 2.18 percent (i.e., 60.6 × 0.036). The peak Ka-band efficiency and uncertainty at f1 correspond to a peak gain of 78.97 dBi ± 0.16 dB.

VII. Efficiency Measurements: Ka-Band at f3

The Ka-band R&D microwave test package was moved to the f3 focal point after the X-band f3 calibrations. The initial tracks focused on refining the subreflector offset curve determined at f1. The optimization procedure used at f1 was automated in the automatic boresighting computer. Two days of star tracking yielded the final total subreflector-commanded position curves (labeled f3) shown in Fig. 2. The best-fit coefficients to the offset curves were input to an APC model file so that the offsets could be automatically applied during tracking operations. This is analogous to the pointing calibration and model determination. The final 2 days of tracking (DOY 174–175) provided the most stable and repeatable measurements for calibration. The zenith attenuation values for these 2 days, computed from SPC-10 weather recordings, varied from 0.10 to 0.12 dB, indicating a drier period than during the Ka-band measurements at f1. The best-fit efficiency curve and the adjusted data points for Ka-band at f3 are shown in Fig. 6.

The Ka-band peak efficiency at f3 was calculated to be 57.02 percent at an elevation angle of 42.0 deg. This is a decrease of 3.6 percent from the peak Ka-band f1 efficiency. The uncertainty ratio, $\sigma_{\eta(el)}/\eta(el)$, for the efficiency measurements is shown in Fig. 7. The uncertainty, σ_η, on the peak efficiency of 57.02 percent at 42.0 deg is 2.51 percent. This corresponds to a peak gain of 78.70 dBi ± 0.20 dB.

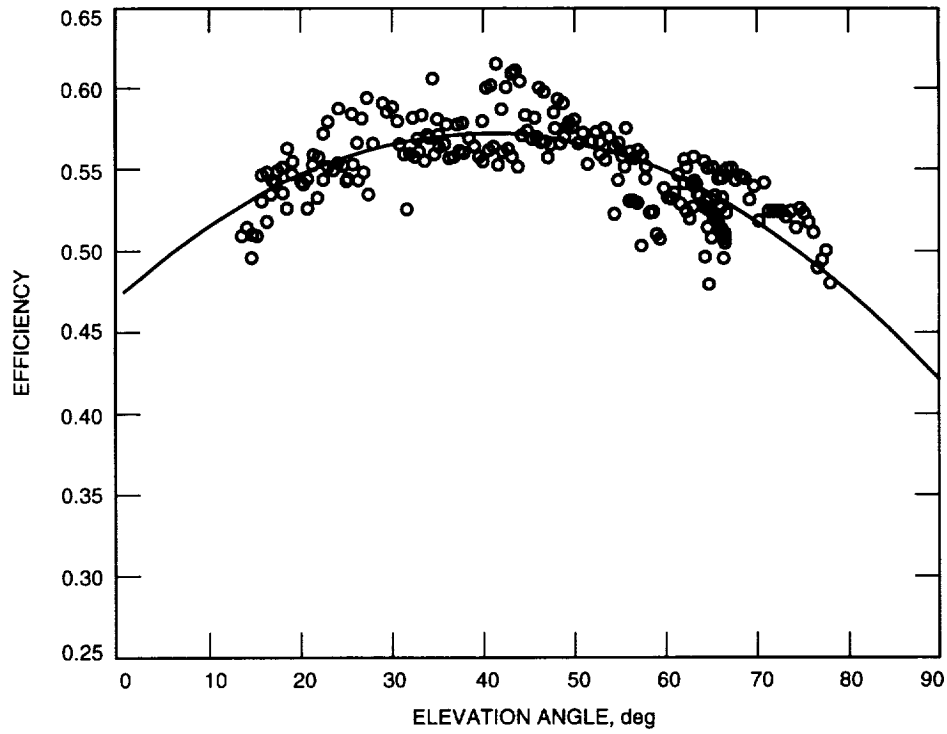

Fig. 6. DSS-24 32-GHz efficiency at the f3 focal point, without atmosphere.

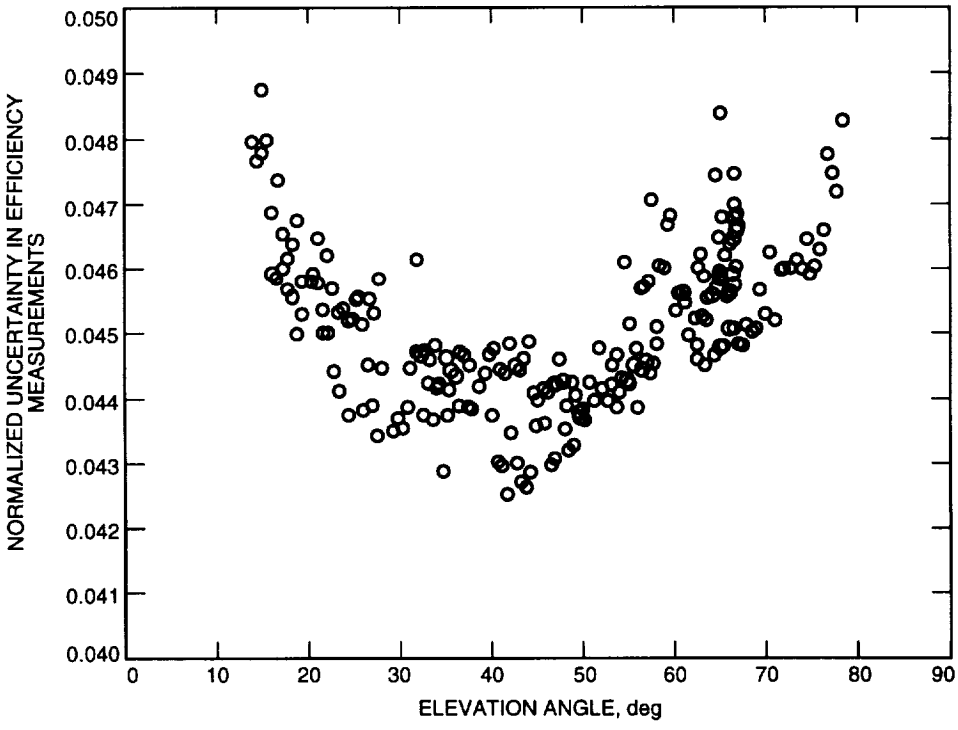

Fig. 7. DSS-24 32-GHz normalized efficiency uncertainty ($\sigma_\eta(el)/\eta(el)$) at the f3 focal point, without atmosphere.

The measurement errors, in general, are larger at f3 due to the decreased antenna gain and the apparent increase in the radio-source temperature measurement noise. The increased spread in the data in Figs. 6 and 7 is due to an azimuth dependence of the efficiency caused by a small beam-waveguide mirror misalignment. For the R&D feed location in the DSS-24 pedestal room (azimuth position = 180 deg), the efficiency is slightly higher for sources with declinations greater than 35 deg rising and setting in the north. The curve fit in Fig. 6 is computed from the combined data sets of 3C274 and 3C84. The efficiency measurements on the northern-passing 3C84 (with peak elevation of 79 deg) almost all lie above the best-fit curve, while those of the southern-passing 3C274 (with peak elevation of 67 deg) are equal to or lie below it.

A. Ka-Band Gravity Loss Analysis

The gravity-induced roll-off of the f3 efficiency curve shown in Fig. 6 is flatter than that measured at f1 (shown in Fig. 4). This is expected since the final subreflector offset curves determined at f3 with the automated subreflector optimization scheme provided better focusing than those used at f1. To quantify the performance increase, Fig. 8 presents the difference of the computed f3 and f1 Ka-band gain curves after the f3 curve has been raised by 0.27 dBi to account for the difference in the measured peak gains. As seen, the low-elevation antenna gravity performance at f3 is superior to that at f1 (e.g., 0.3 dBi greater at a 10-deg elevation). Thus, only the f3 efficiency curve should be used to predict the efficiency degradation as a function of elevation angle. The f3 gravity loss profile, computed from the best-fit efficiency curve, is shown in Fig. 9. It is assumed that there is zero loss at the peak gain elevation angle of 42 deg. Note that the asymmetry of the gravity loss curve is more probably due to an artifact of the differing profiles of the individual radio-source efficiency measurements, as discussed above, than to errors in the experimentally determined high-elevation angle subreflector focusing curves.

VIII. Efficiency Measurements: X-Band Operational Feed

Efficiency measurements at f3 were made on the X-band operational feed with the S-/X-band dichroic plate installed for the 3 days of 207–209. During this period, the computed zenith attenuation varied from 0.034 to 0.038 dB. The adjusted efficiency data points are shown in Fig. 10.

On the X-band operational feed, the noise temperature measurements were taken at the input of the downconverter. However, as seen in Fig. 10, gain instability was a problem during the measurements. It was determined that the X-band maser was stable to ± 0.1 dB, corresponding to a 0.2-K noise temperature measurement stability on the principal calibrator, 3C274. Thus, at any elevation angle, the measurement noise on the efficiency measurements was 1.5 to 2 percent alone, rendering a quadratic curve fit impractical. The peak efficiency was estimated by averaging the data points between 42 and 48 deg. The peak efficiency on the X-band operational feed was computed to be 71.10 percent with an estimated uncertainty of 2.30 percent. This corresponds to a peak X-band gain for the operational feed of 68.09 dBi ± 0.14 dBi.

IX. Efficiency Measurements: S-Band Operational Feed

S-band efficiency measurements were made on the operational feed on DOY 186–188. The radio sources tracked were 3C274 and 3C123, both southern-passing targets. Figure 11 shows the measurements, corrected for atmospheric absorption with an average zenith attenuation value of 0.03 dB, as a function of elevation angle. The azimuth angles for the data points range from 60 to 295 deg, with southern (180-deg azimuth) transit elevation angles of 67.5 deg for 3C274 and 83 deg for 3C123. The peak S-band efficiency was computed to be 71.50 percent, measured for both sources at the 180-deg azimuth angle. The uncertainty on the peak value is 1.82 percent, which corresponds to a peak S-band gain of 56.79 dBi ± 0.11 dB.

The variation of antenna efficiency as a function of azimuth angle shown in Fig. 11, with the peak operational gain at the 180-deg azimuth, was predicted by rf analysis for the S-band feed in the 270-deg

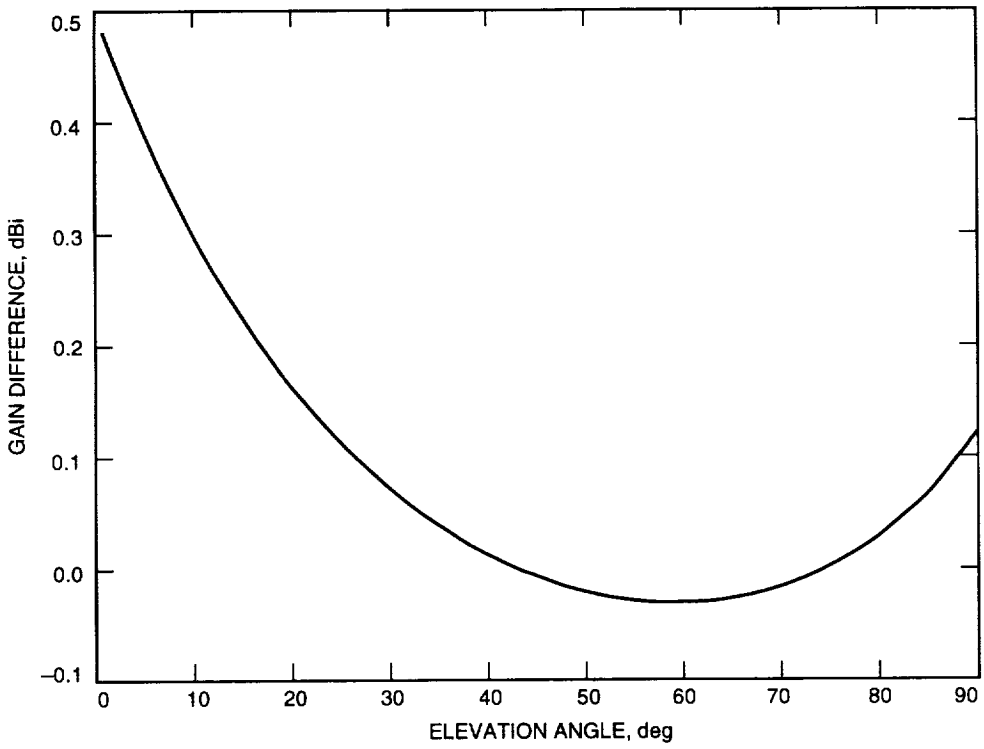

Fig. 8. The difference of normalized f3 and f1 gain curves.

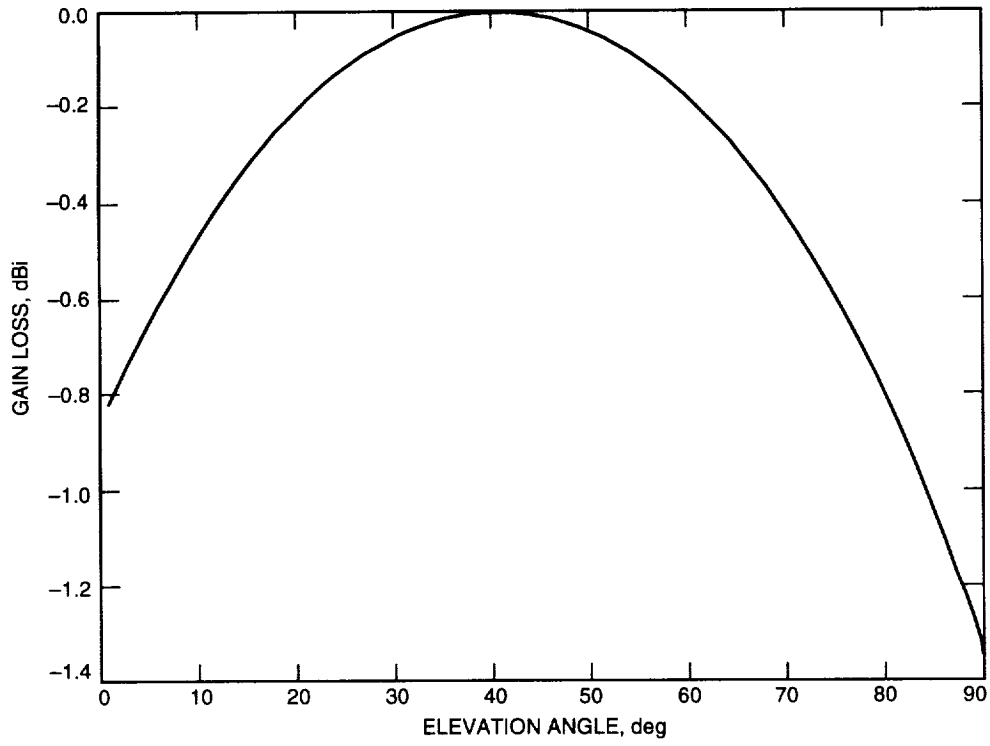

Fig. 9. DSS-24 32-GHz gravity loss for the f3 focal point.

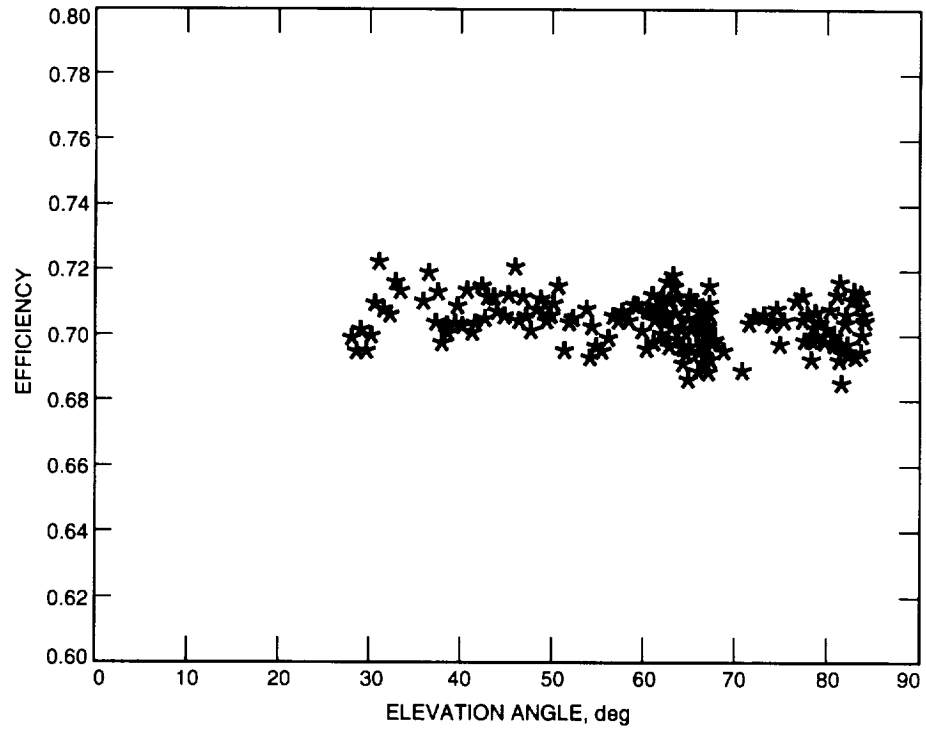

Fig. 10. DSS-24 8.45-GHz efficiency measurements on the operation feed at the f3 focal point, without atmosphere.

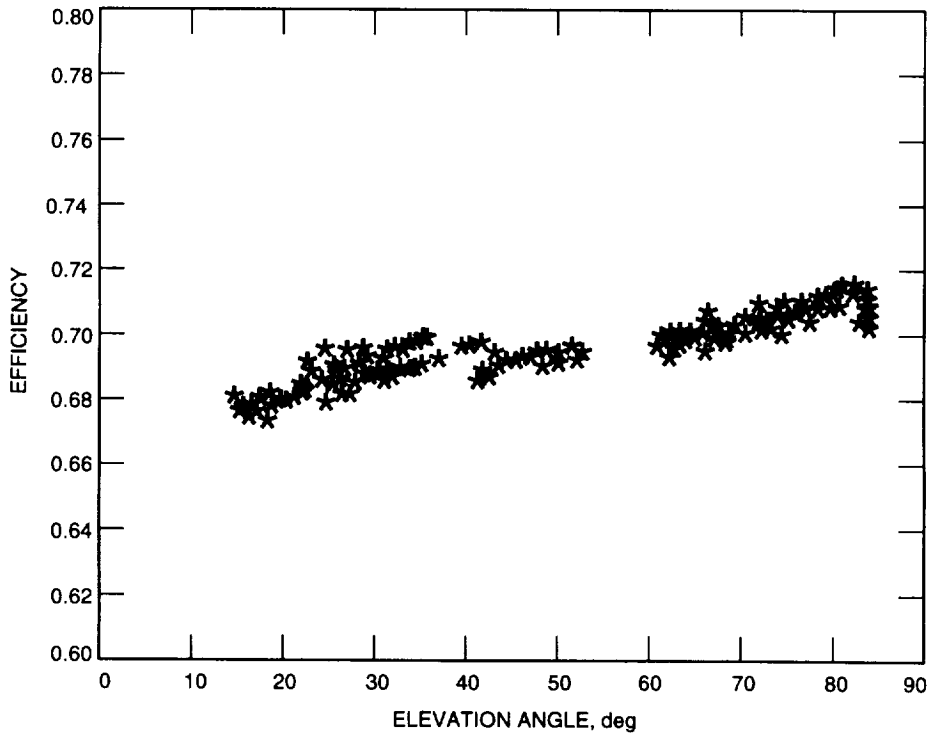

Fig. 11. DSS-24 2.295-GHz efficiency measurements on the operational feed at the f3 focal point, without atmosphere.

pedestal room position.[9] The predicted antenna efficiency variation between the azimuth range of 60 to 295 deg, computed for a perfectly aligned beam-waveguide mirror system, was 2 percent. As measured at DSS 24 and shown in Fig. 11, the variation is 4 percent over the same angle range.

X. Summary of Results

The aperture efficiency of the DSS-24 34-m beam-waveguide antenna has been calibrated at the S- (2.295-GHz), X- (8.45-GHz) and Ka-band (32-GHz) frequency bands. Table 2 presents a summary of the peak gains and efficiencies measured during the rf performance evaluation period. The uncertainties on the peak values are also given and are based on a propagation of measurement errors and radio-source flux and size correction errors. Table 3 gives the best-fit second-order polynomial coefficients for the X- and Ka-band efficiencies measured on the R&D feed packages. The first four peak gain and efficiency estimates in Table 2 were computed from these coefficients. The S- and X-band peak values measured on the operational feeds were derived by averaging the measurements in a small angular range about the observed peak efficiency angles. The Ka-band gravity loss as a function of elevation angle was computed from the best-fit DSS-24 f3 efficiency curve and is shown in Fig. 9. The final y- and z-axis subreflector (total) offset curves experimentally determined at the f3 focus are presented in Fig. 2 and have been left in the DSS-24 antenna-pointing controller for future tracking operations.

Table 2. Summary of DSS-24 antenna peak gains and efficiencies at the S-, X-, and Ka-band frequencies.

Frequency, GHz, and focal point	Gain, dBi	1-sigma gain error, dB	Efficiency, percent	1-sigma efficiency error, percent
8.45 at f1	68.33	0.12	75.25	2.04
8.45 at f3	68.19	0.11	72.67	1.81
32 at f1	78.97	0.16	60.60	2.18
32 at f3	78.70	0.20	57.02	2.51
8.45 operational feed at f3	68.09	0.14	71.10	2.30
2.295 operational feed at f3[a]	56.79	0.11	71.50	1.82

[a] Measured at azimuth angle = 180 deg.

Table 3. Best-fit second-order polynomial coefficients for S- and Ka-band efficiencies, without atmosphere, measured on the R&D feed packages.

Efficiency	Efficiency model = $c_0 + c_1 el + c_2 el^2$ where el = elevation angle, deg		
	c_o	c_1	c_2
X-band at f1	0.748067	0.000211491	−0.00000250421
X-band at f3	0.714972	0.000457441	−0.00000444267
Ka-band at f1	0.442223	0.00737073	−0.0000827938
Ka-band at f3	0.466983	0.00504885	−0.0000618488

[9] W. Veruttipong, "S-Band Efficiency and G/T Performance Performance for Various Azimuth Positions," JPL Interoffice Memorandum 3327-94-113 (internal document), Jet Propulsion Laboratory, Pasadena, California, June 9, 1994.

Acknowledgments

S. D. Slobin is gratefully acknowledged for his technical input and recommendations. The authors thank M. Wert and R. Littlefair for providing weather measurement data from SPC 10 and DSS 13, respectively.

References

[1] S. D. Slobin, T. Y. Otoshi, M. J. Britcliffe, L. S. Alvarez, S. R. Stewart, and M. M. Franco, "Efficiency Calibration of the DSS 13 34-Meter Beam-Waveguide Antenna at 8.45 and 32 GHz," *The Telecommunications and Data Acquisition Progress Report 42-106, April–June 1991*, Jet Propulsion Laboratory, Pasadena, California, pp. 283–297, August 15, 1991.

[2] L. S. Alvarez, "Analysis and Applications of a General Boresight Algorithm for the DSS-13 Beam-Waveguide Antenna," *The Telecommunications and Data Acquisition Progress Report 42-111, July–September 1992*, Jet Propulsion Laboratory, Pasadena, California, pp. 48–61, November 15, 1992.

[3] S. R. Stewart, "DSS-13 Beam-Waveguide Antenna Performance in the Bypass Mode," *The Telecommunications and Data Acquisition Progress Report 42-108, October–December 1991*, Jet Propulsion Laboratory, Pasadena, California, pp. 135–153, February 15, 1992.

[4] P. H. Richter and S. D. Slobin, "DSN 70-Meter Antenna X- and S-Band Calibration, Part I: Gain Measurements," *The Telecommunications and Data Acquisition Progress Report 42-97, January–March 1989*, Jet Propulsion Laboratory, Pasadena, California, pp. 314–351, May 15, 1989.